Quantification of the Effects of Recombination and Injection in the Performance of Dye-Sensitized Solar Cells Based on *N*-Substituted Carbazole Dyes

Eva M. Barea,*,† Ceylan Zafer,*,‡ Burak Gultekin,‡ Banu Aydin,‡ Sermet Koyuncu,§ Siddik Icli,‡ Francisco Fabregat Santiago,† and Juan Bisquert†

Photovoltaic and Optoelectronic Devices Group, Physics Department, Universitat Jaume I, 12071 Castello, Spain, Solar Energy Institute, Ege University, TR-35100 Izmir, Turkey, and Çan Vocational School, Çanakkale Onsekiz Mart University, 17400, Çanakkale, Turkey

Received: June 17, 2010; Revised Manuscript Received: September 29, 2010

Two new sensitizers for dye sensitized solar cells have been designed consisting of thiophene units asymmetrically functionalized by *N*-aryl carbazole. The di(tert-butyl) carbazole moieties acts as an electron donor group, the thiophene chain as a bridge group, and the cyanoacrylic acid as an anchoring and electron acceptor group. An increase of the conjugation length produces two main effects: first, it leads to a red-shift of the optical absorption of the dyes, resulting in an improved overlap of the absorption with the solar spectrum. Second, the oxidation potential decreases. The photovoltaic performance of this set of dyes as sensitizers in mesoporous TiO_2 solar cells was investigated using electrolytes containing the iodide/triiodide redox couple. The dye with the best absorption characteristics showed the highest photocurrent but lower open circuit voltage due to more losses by recombination. A trend between structure (molecule dyes size) and recombination is demostrated using an analysis procedure based on β-recombination model that combines impedance spectroscopy and density current−voltage data.

1. Introduction

Dye sensitized solar cells (DSCs) based on molecular-sensitized nanostructured metal oxides have attracted significant attention as low-cost photovoltaic devices.[1] The photosensitizer plays important roles in determining the stability, light-harvesting capability, and also the total cost of DSCs. Presently the most important photosensitizers are Ruthenium dyes,[2,3] yielding overall AM 1.5 solar to electric power conversion efficiencies up to 11.3%.[4] But the high cost of ruthenium, the necessity of purification treatments, and the low molar extinction coefficients makes the research on alternative, metal-free organic dyes appealing for their application in large DSC modules.

Organic sensitizers have the advantage of high extinction coefficients and can thus also meet the demand of good light-harvesting efficiency with thinner TiO_2 films. Less volatile redox systems such as ionic liquids[5−7] and hole conductors[8−10] require thinner TiO_2 films because of mass transport limitations or insufficient pore filling. A great variety of organic sensitizers based on polyene-triphenylamine,[11−17] coumarin,[13,18,19] and indoline[20−22] moieties give respectable conversion efficiencies of 5−9%[23] with the traditional iodide/triiodide redox system. Despite the promising results obtained so far, more research is needed to understand the energetic, kinetic, and geometric interplay between dye, semiconductor framework, and electrolyte to design efficient and stable organic dyes for large scale applications.

In this study two new organic dyes, BG-1 and BG-2, based on the push−pull concept, have been tested. As shown in Figure 1 the dyes contain either one (BG-1) or two (BG-2) thiophene units that act as a bridge between the electron donor group, di(tert-butyl) carbazole moieties, and the anchoring and electron acceptor group, cyanoacrylic acid. On the basis of previous experience on DSC characterization by impedance spectroscopy (IS),[24] it is possible to provide a detailed understanding of the factors determining the device performance. Here we report on the relation between charge-transfer resistance and capacitance of the cell, measured by IS, with the $j-V$ curves under 1 sun illumination. We apply a new approach based on nonlinear beta recombination model ($U_n = k_r n^{\beta}$)[25,26] that captures the essential features of recombination in a DSC. We describe here a simple but powerful method to treat simultaneously the recombination resistance and the $j-V$ curve. This provides a detailed account of the DSC behavior with the different sensitizers. The most challenging aspect of the analysis is to separate the change of conduction band position from an array of charge-transfer kinetics factors. This is not trivial since surface changes induced by the presence of the dye may affect both the β-parameter that modifies the fill factor[27] and the charge-transfer kinetics rates by surface blocking or other variations of the interfacial kinetic.[28,29] Our results allow to discriminate some of these factors and confirm that IS is a predominant technique to obtain a comprehension of the processes involved in DSC.

2. Experimental Section

Synthesis and Characterization of BG-1 and BG- 2 Dyes. The synthetic approach of BG-1 and BG-2 is outlined in Scheme 1.

First, 3,6-ditert-butyl-9H-carbazole (**1**) was synthesized by using Fridel-Crafts alkylation according to published procedure by Gibson et al.[30]

3,6-Di-*tert*-butyl-9-(4-iodophenyl)-9H-carbazole (**2**) was synthesized by an Ullman-type condensation of **1** and excess amount of 1,4-diiodobenzene in dimethylamine in the presence of CuI as a catalyst and K_2CO_3. The pale-yellow solid was

* To whom correspondence should be addressed. E-mail: barea@fca.uji.es (E.M.B.); ceylan.zafer@ege.edu.tr (C.Z.).
† Universitat Jaume I.
‡ Ege University.
§ Çanakkale Onsekiz Mart University.

10.1021/jp1055842
Published on Web 11/03/2010

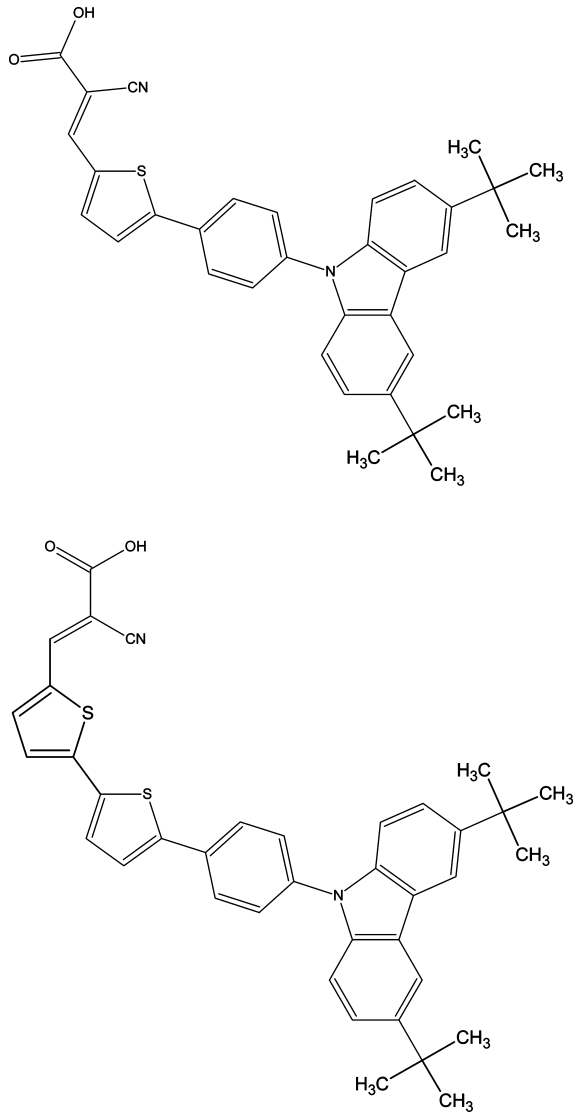

Figure 1. Chemical structure of BG-1 (top) and BG-2 (bottom).

purified by column chromatography in a good yield of 80%. Then, 3,6-di-*tert*-butyl-9-[4-(2-thienyl)phenyl]-9H-carbazole (**3**) was synthesized by using the palladium-catalyzed Suzuki coupling reaction; **3** reacted with 2-thiopheneboronic acid. For addition of the second thiophene units on **3**, first **3** was brominated with the NBS and then coupled to the second thiophene unit by using previous procedure to give **4** and **7**, respectively. The first and second reaction yields were found to be 80 and 75%, respectively. The carbazole-thiophene compounds (**3** and **7**) were formulated by using Vismayer−Heck reaction in the presence of the $POCl_3$. The final step was a Knoevenagel condensation with cyanoacetic acid to convert carbaldehydes to cyanoacrylic acids. All final products were purified by column chromatography to give reddish products. The initial compounds and products were fully characterized by ^1H and ^{13}C NMR (not shown). The reaction details of the products are explained in the Supporting Information.

Electrochemical properties of BG-1 and BG-2 were studied by cyclic voltametry (CV). CV measurements were recorded by a CH 660B model potentiostat from CH Instruments in a three-electrode cell consisting of a platinum wire counter electrode (CE), a glassy carbon electrode used as a working electrode (WE), and a Ag/AgCl electrode in 3 M KCl (aq) used as a reference electrode (RE). Measurements were carried out in 0.1 M $TBAPF_6$ in acetonitrile as supporting electrolyte. The sweep rate was kept constant at 0.1 V/s. The ferrocene/ferrocenium redox couple was used as an internal reference which was exhibited oxidation potential at +0.41 V.

DSC Preparation. DSCs were fabricated using TiO_2 nanocrystalline paste prepared by hydrolysis of titanium tetraisopropoxide[1] with the addition of ethyl cellulose as a binder in α-terpineol. The TiO_2 layers were deposited with the doctor blading technique on transparent conducting oxide (TCO) glass (Pilkington TEC15, ∼15Ω/sq resistance). The resulting photoelectrodes of 10-μm thickness were sintered at 450 °C and then immersed in 0.04 M $TiCl_4$ solution for 30 min at 70 °C followed by calcination at 450 for 30 min to obtain good electrical contact between the nanoparticles. When the temperature decreased to 40 °C all the electrodes were immersed in dye solution (0.3 mM in chloroform:methanol (1:1)) overnight (16 h). After the adsorption of the dye, the electrodes were rinsed with the same solvent. The solar cells were assembled with the counter electrode (thermally platinized TCO) using a thermoplastic frame (Surlyn 25 μm thick). Redox electrolyte (0.5 M LiI (99.9%) and 0.05 M I_2 (99.9%) in 3-methoxypropionitrile) was introduced though a hole drilled in the counter electrode that was sealed afterward. Prepared solar cells (0.5 cm^2 size, masking solar cell to 0.35 cm^2) were characterized by $j-V$ characteristics and IS. Photocurrent and voltage were measured using a solar simulator equipped with a 1000-W ozone-free Xenon lamp and AM 1.5 G filter (Oriel), where the light intensity was adjusted with an NREL-calibrated Si solar cell with a KG-5 filter to 1 sunlight intensity (100 mW cm^{-2}). IS measurements were carried out under an irradiation of 1 sun (AM 1.5 conditions) and different bias potentials that ranged from zero to open circuit potential and frequencies between 1 MHz and 0.1 Hz.

3. Result and Discussions

Synthesis and Characterization. The absorption spectra of the BG-1 and BG-2 dye both in chloroform solution and adsorbed on the transparent mesoporous TiO_2 films are shown in Figure 2. The absorption maximum (λ_{max}) of BG-2 exhibited a 30 nm batochromic shift associated with the bonding of one more thiophene to the BG-1 dye. Therefore, the number of the thiophene moieties affects the low energy edges and also band gap of the dyes. The intersect of the absorption and fluorescence spectra (not shown) for BG-1 is at 509 nm and for BG-2 is 532 nm, which corresponds to band gap of 2.440 and 2.330 eV, respectively. The molar absorption coefficients, ε at λ_{max}, were 71000 and 73200 M^{-1} cm^{-1} for BG-1 and BG-2, respectively. The UV−vis spectra on TiO_2 has been integrated and the maximum current that the dyes give are 11.10 mA/cm^2 for BG-1 and 11.75 mA/cm^2 for BG-2.

That result is well correlated with the j_{sc} that provide the cells prepared, which has been inferior due to the recombination process. That result indicates that for BG-1 in injection is around 76% and for BG-2 is near 93%. Figure 3 shows the calculated molecular structure of BG-1 and BG-2 dyes and the electron distribution of the highest-occupied molecular orbital (HOMO) and lowest-unoccupied molecular orbital (LUMO) using Hyperchem with semiempirical AM1 equations. Calculations indicate that the HOMO is distributed along the thiophenes chain and the LUMO is located over the cyanoacrylic unit through thiophene chain. This distribution suggests the existence of charge transfer from the donor (carbazole and thiophenes) to the acceptor (cyanoacrylic acid) units.

Spectroscopic data have been summarized in Table 1. The electrochemical redox behavior of BG-1 and BG-2 has been

SCHEME 1: Synthesis Route of BG-1 and BG-2

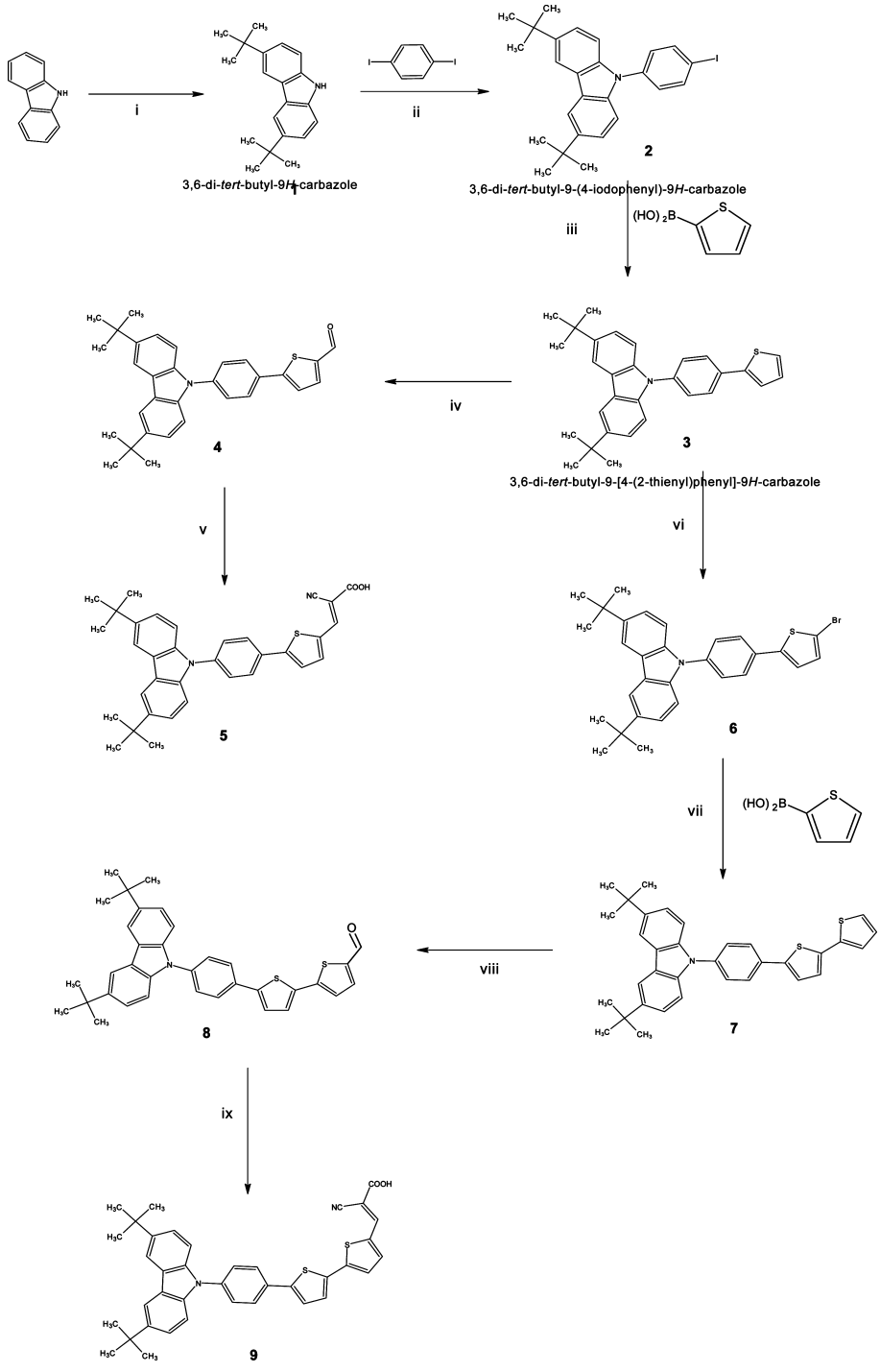

studied by CV in acetonitrile solution (Figure 1 of Supporting Information). BG-1 and BG-2 exhibit two distinct oxidation states. For both molecules, the first oxidation peak at 1.27 V is attributed to the oxidation of carbazole. The second peak at about 1.76 V is ascribed to thiophene moiety of BG-1. For BG-2, due to the longer π-conjugation, the oxidation peak is shifted to lower potential to about 1.48 V. On the other hand, the quasireversible reduction peak of BG-1 and reversible reduction of BG-2 attributed to cyanoacrilic acid moiety was observed at about $E_{1/2} = -1.30$ and -1.44 V, respectively. Finally the HOMO energy level was calculated by using oxidation onset of BG dyes, and LUMO energy levels were estimated by using optical band gap (E_g) calculated from the intersect of fluorescence emission and absorption spectra and then using expression $E_{LUMO} = E_{HOMO} - E_g$ (Table 1). The estimated LUMO levels of the two dyes are sufficiently higher than the electron injection level of TiO_2 (ca. -0.5 V vs NHE) for effective electron injection, while their HOMO levels are sufficiently lower than electrolyte pair I^-/I_3^- (ca. 0.4 $-$ 0.5 V vs NHE) to facilitate regeneration of the oxidized dye.

Solar Cell Study. DSC devices, using BG-1 and BG-2 sensitizers, were characterizated by $j-V$ curves and compared with N719 as a reference, see Figure 4. The first rows of Table 2 show the main parameters obtained from the $j-V$ characterization. It should be remarked that electrolyte conditions (the same in the three cells) have been optimized for the two new organic dyes tested, BG-1 and BG-2, as a result the performance of N719 dye in this configuration is not high. However, with

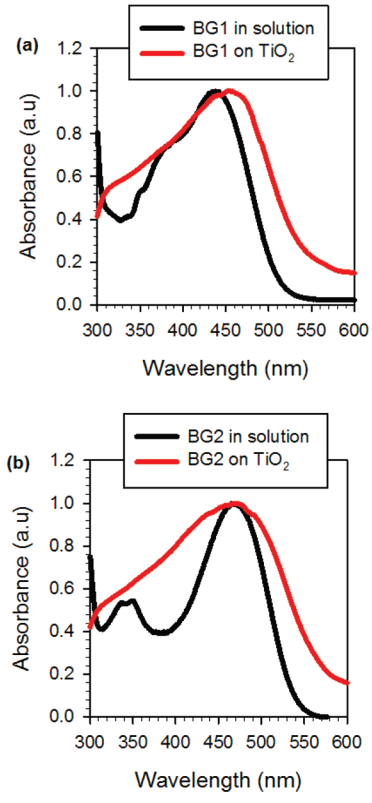

Figure 2. UV−vis spectra of (a) BG-1 in chloroform and adsorbed on transparent TiO_2 film and (b) BG-2 in chloroform and adsorbed on transparent TiO_2 film.

the same DSC preparation protocols, a solar cell of good performance at 1 sun can be obtained. This is shown in Figure 2 of Supporting Information where we compare the performance of two cells with N719 dye. For the cell with lower photocurrent (N719) the electrolyte composition and the fabrication conditions are the same as those mentioned in the Experimental section. And for the high-performance cell (N719-op), the electrolyte composition is 0.03 M I_2, 0.6 M 1-*butyl*-3-methylimidazolium iodide, 0.10 M guanidinium thiocyanate, 0.5 M 4-*tert*-butylpyridine in acetonitrile:valeronitrile (85:15 v/v); the photoelectrode consists of a double layer, transparent layer 8 μm thick and scatter layer of 4 μm, and the absorption time was 16 h. It should be remarked the important role played by the electrolyte composition, since all the performance parameters of the cell are improved and the efficiency increases from 3.90 to 7.20% (see Table 1 of Supporting Information).

From the data shown in Figure 4 and Table 2, it is clearly observed that for BG-2 dye (with two thiophenes units) the injection current is higher, in good correlation with our previous studies,[31] because the light harvesting is higher for BG-2 dye (see UV−vis spectra in Figure 2). Nevertheless, the overall conversion efficiency is similar to that of BG-1. Clearly BG-1 provides a larger photovoltage than BG-2 that compensates the lower extent of photon absorption. There is a variety of causes for this, i.e., an upward shift of the conduction band of TiO_2, E_c, or a decrease of the rate of recombination, since it has been observed that organic dyes exert a strong influence on the rate of charge transfer.[32] To clarify these assumptions, IS measurements were performed on the DSCs at different bias potentials and 100 mW cm^{-2} light intensity (simulated AM 1.5 global radiation). These measurements were analyzed using the impedance model developed by Bisquert and Fabregat[24,33] that allows to isolate the recombination resistance from other resistive contributions in the cell. Parts a and b of Figure 5 show the measured capacitance, C_μ, and recombination resistance, R_{rec}, as a function of the potential, for the different cells. The chemical capacitance describes the density of states in the band gap of TiO_2[34] and the recombination resistance is related to recombination current, j_{rec}, as follows[35]

$$R_{rec} = \left(\frac{\partial j_{rec}}{\partial V}\right)^{-1} \quad (1)$$

The analysis of R_{rec} provides information about the extent of recombination in each solar cell. However, as mentioned above the change of dye can also produce a change of the energetics, i.e., of the conduction band of TiO_2 semiconductor, E_c, with respect to the redox energy in the electrolyte, E_{F_0}. As observed

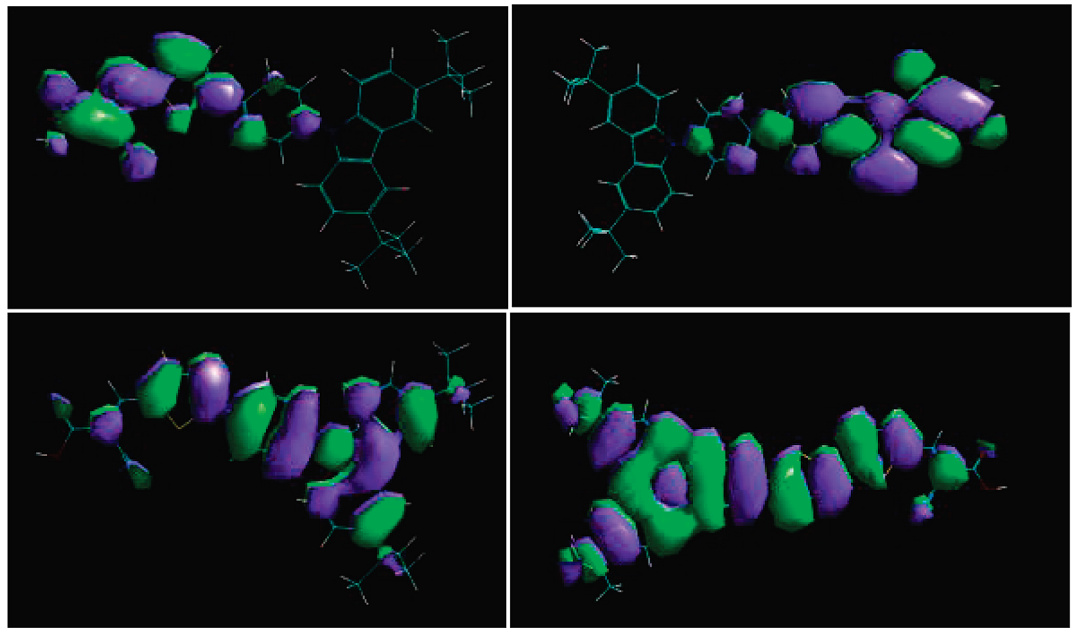

Figure 3. Optimized chemical structures and frontier molecular orbitals of BG-1 (left) and BG-2 (right) at HOMO (lower) and LUMO (upper).

TABLE 1: Optical and Electrochemical Properties of BG-1 and BG-2 Dyes

dye	λ_{abs}* (nm)	ε (M^{-1} cm^{-1})	λ_{em}* (nm)	E_{0-0} (eV)	E_{ox} (V)	E_{red} (V)	E_{LUMO} (eV)	E_{HOMO} (eV)
BG-1	438	71000	585	2.44	+1.27	−1.30	−3.22	−5.66
					+1.76	−1.52		
BG-2	468	73200	589	2.33	+1.27	−1.44	−3.33	−5.66
					+1.48	−1.72		

in the chemical capacitance values reported in Figure 5b the conduction band edge of titania is lower for BG-2 (the meaning of voltage V_F is explained below, essentially V_F corresponds to remove from the bias voltage the effect of ohmic drops in the solar cell). The lower position of the conduction band facilitates the electron injection from the dye and tends to increase the photocurrent.

In principle if the dye excited state is sufficiently high above the titania conduction band, one might not expect and increase of the photocurrent when the conduction band is shifted downward. However, we have observed in measurements that bringing down the conduction band continuously increases the photocurrent, for cells with high collection efficiency, and this means that injection at the titania surface is increased. To corroborate this point, we have prepared cells using N719 sensitizers under the same condition and three different electrolyte compositions:

DSC A: 0.6 M 1-butyl-3-methylimidazolium iodide, 0.03 M I_2, 0.10 M guanidinium thiocyanate, 0.50 M 4-*tert*-butylpyridine in methoxypropionitrile.

DSC B: 0.5 M LiI, 0.05 M I_2, 0.50 M 4-*tert*-butylpyridine in methoxypropionitrile.

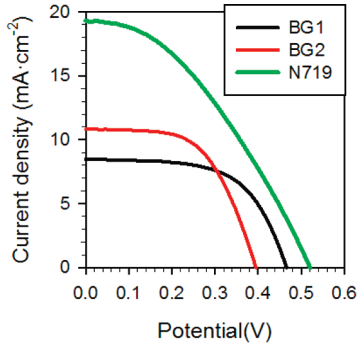

Figure 4. $j-V$ curves of DSCs sensitized with BG-1, BG-2, and N719 under standard conditions (100 mW cm^{-2}, AM 1.5).

TABLE 2: Photovoltaic Performances of the DSCs Sensitized with BG-1, BG-2, and Reference Dye N719 and Parameters Obtained by Combination of Both j−V and Impedance Data

sample	BG-1	BG-2	N719
V_{oc} (V)	0.47	0.40	0.52
j_{sc} (mA/cm^2)	8.47	10.9	19.3
FF	0.60	0.57	0.38
η (%)	2.39	2.48	3.90
β	0.51	0.60	0.42
j_o (mA/cm^2)	1.26×10^{-3}	1.22×10^{-3}	1.68×10^{-3}
j_{ok} (mA/cm^2)	280	1329	40
R_{series} (ohm)	20	25	26
$FF_{(i)}$	0.67	0.67	0.66
$\eta_{(i)}$ (%)	2.66	2.92	6.63

Values of V_{oc}, FF, j_{sc}, and efficiency are obtained at steady state measurement under 100 mW cm^{-2} light intensity and AM 1.5 global radiation. β is a recombination parameter, j_o a dark current, j_{ok} the charge-transfer constant, R_{series} is the series resistance (given a constant value to simplify the analysis), and internal (i) FF and efficiency are calculated without effect of series resistance.

DSC C: 0.5 M LiI, 0.05 M I_2 in methoxypropionitrile).

The cells where characterized by $j-V$ curves measured under 1 sun illumination and by IS (Supporting Information). The results clearly indicate that for DSC A (with ionic liquid (IL) and basic additives in the electrolyte) the open circuit potential is high (0.78 V), meanwhile the j_{sc} is low (12.31 mA/cm^2), which means a high position[36,37] of the E_c that affects the driving force of the electron injection in agreement with IS results where the value of capacitance is low. The DSC B presents 10 mV less for V_{oc} and the photocurrent increases (17.20 mA/cm^2) due to the electrolyte composition containing just a basic additive (4-*tert*-butylpyridine) without IL. Thus a moderate downward shift of E_c of titania occurs, and the driving force of the injection is higher than DSC A. In that case the capacitance of the cell is higher (Figure 3b, Supporting Information). Finally, if no basic additive is included in the electrolyte composition (DSC C) the E_c of titania is shifted downward, which produces a decrease in the value of V_{oc} (0.52 V) and increasing the j_{sc} (19.30 mA/cm^2) because the driving force in that case is higher and there is an increase in the capacitance[38] (Supporting Information). In addition to displacement of the conduction band of the semiconductor, the effect of the electrolyte composition in the FF and overall conversion efficiency is related with the role that the additives play in the recombination process. IL and basic additives such as 4-*tert*-butylpyridine make a blocking layer on the titania surface, decreasing the back recombination of the injected electrons, increasing the value of the FF and improving the overall conversion efficiency of the cell. In the case of inclusion of IL in the composition of the electrolyte there are other factors that could affect the FF and efficiency like the diffusion of redox species toward the counterelectrode.

Turning back to the organic sensitizers studied in this work, we observe that wider absorption range of BG-2 in conjunction with the lower position of the conduction band of TiO_2 readily explains the higher current obtained for this dye in comparison with BG-1, as observed in Figure 4.

The explanation of the changes of photovoltage is however more complex. Many papers in the literature approach this question by comparing certain kinetic quantities such as the electron lifetime.[29] However, the photovoltage is also influenced by the amount of injected charge. Aiming to a more quantitative understanding of the different performances of the studied dyes, we propose here a model that allows analysis of both IS results and $j-V$ curve in combination to provide all the performance and recombination parameters in the framework of a relatively simple kinetic scheme. We construct the diode model describing $j-V$ curves from the β-recombination model, in which the recombination rate is given by the expression

$$U = k_r n_c^{\beta} \qquad (2)$$

as recently discussed.[25,26]

The generation by incident light of photon flux Φ_0 occurs at a rate $G = \Phi_0/L$ per unit volume, being L the thickness of the absorber layer. A more complex expression for generation rate

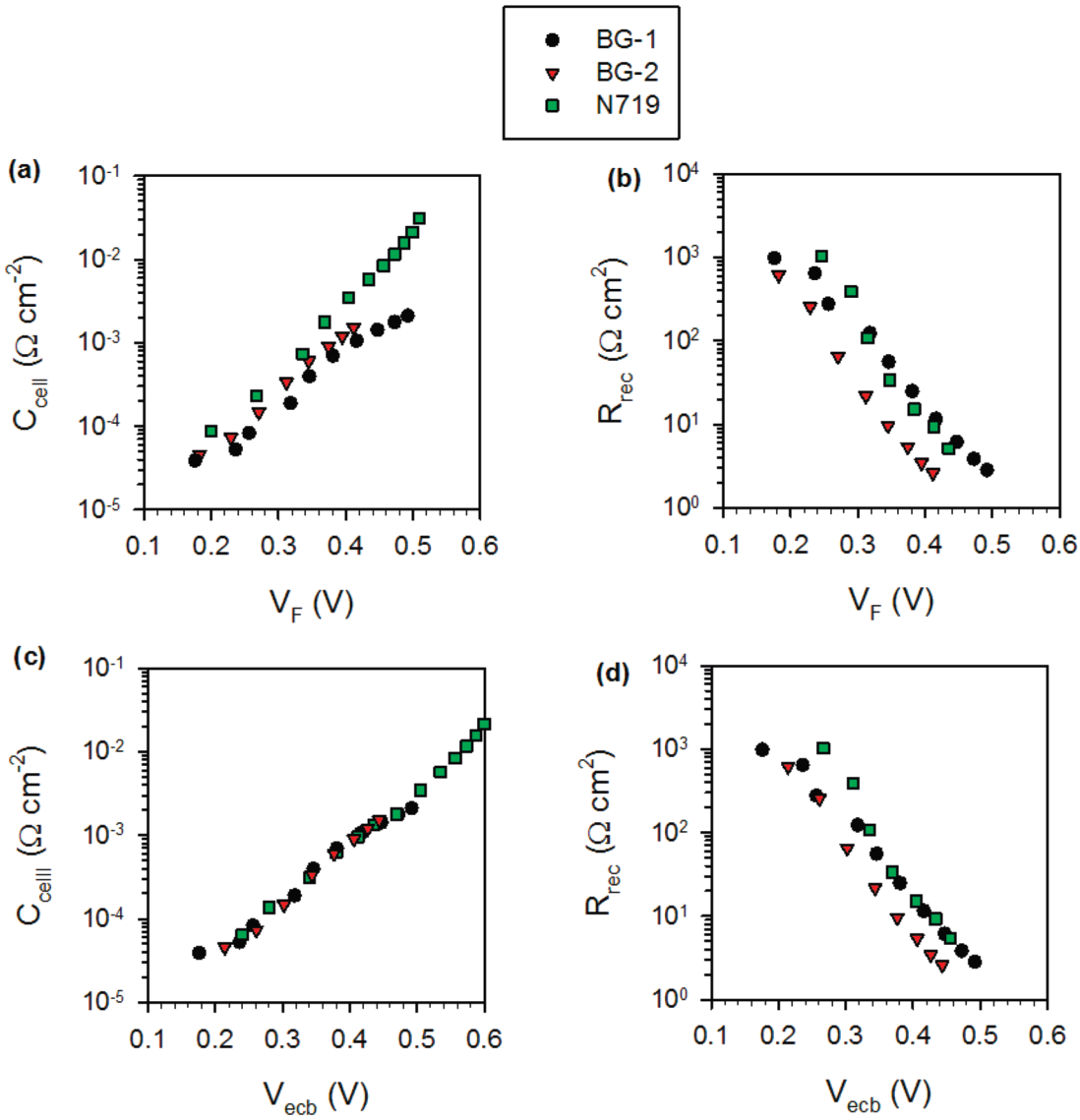

Figure 5. Capacitance (a) and recombination resistance (b), obtained from IS of the solar cells with BG-1, BG-2, and commercial N719 as sensitizers under illumination (100 mW cm^{-2}, AM1.5), with respect to Fermi level voltage (without the effect of series resistance). (c) Capacitance and (d) recombination resistance replotted with respect to equivalent common conduction band voltage so that distance between Fermi level and conduction band is the same in all cases.

can be introduced if required. The concentration of electrons n is governed by the conservation equation

$$\frac{dn_c}{dt} = G - U + U_0 \tag{3}$$

Here U_0 is a term that provides equilibrium at $G = 0$. The eq 3 assumes that collection efficiency in the cell is high so that diffusion terms are neglected. The increase of the Fermi level, E_{F_n}, in the semiconductor film can be described as a "Fermi level voltage", V_F, as follows

$$V_F = (E_{F_n} - E_{F_0})/q \tag{4}$$

where q is the elementary charge. The free electron density is given by

$$n_c = n_0 e^{qV_F/k_BT} \tag{5}$$

where k_B is Boltzmann's constant, T the temperature, and n_0 an equilibrium density. By integration of eq 3 it can be shown that the current density has the expression

$$j = j_{sc} - j_0(e^{q\beta V_F/k_BT} - 1) \tag{6}$$

Here, j_{sc} is the short-circuit photocurrent. The recombination current has the form

$$j_{rec} = j_0 e^{q\beta V_F/k_BT} \tag{7}$$

According to eq 7 recombination rate is determined by two factors: the dark current parameter j_0 and an exponential increase with V_F, associated with the increasing electron density in the semiconductor. In the model of eq 6, the parameter j_0 contains the kinetic information of charge transfer at nanoparticulate titania surface and requires some discussion.

First, we associate j_0 with the denomination "dark saturation current", which is standard in diode models for semiconductor

devices, in which j_0 can be easily measured in reverse bias mode in the dark, as is obvious in eq 6. However in a DSC in reverse mode we may get other channels for current (for example via the substrate of nanoparticulate electrode) that are *not* included in eq 6. Therefore analysis in reverse bias of a DSC requires modification of eq 6 and in general does not give the parameter j_0.

Second, to compare charge-transfer rates in different DSCs, j_0 is not the best parameter. This is because differences of conduction band energy E_c imply a difference of the equilibrium electron density, n_0, and hence affect j_0. Therefore we introduce a new parameter j_{0k} by the following definition

$$j_0 = j_{0k} e^{-\beta E_c / k_B T} \tag{8}$$

Now j_{0k} is a good representation, from an empirical approach, of the rate constant for recombination (k_r in eq 2). Equation 7 can be expressed as

$$j_{rec} = j_{0k} e^{\beta(qV_F - E_c)/k_B T} \tag{9}$$

The series resistance in the cell, R_s, usually makes a significant effect, especially when the photocurrent is large. The voltage V_F is related to applied voltage (V_{appl}) as

$$V_{appl} = V_F + V_s = V_F + jR_s \tag{10}$$

Finally, by eqs 1 and 7 the recombination resistance is given by the expression[35]

$$R_{rec} = \frac{k_B T}{q\beta j_0} e^{-q\beta V_F / k_B T} \tag{11}$$

The performance of a given DSC is determined by the $j-V$ curve at the required illumination level. But an analysis of the performance requires to discriminate several factors that we have mentioned: series resistance, recombination parameters, etc. These factors are not usually available simply by the analysis of $j-V$ curve data. This is due to a number of reasons, but first of all, recombination rate may depend on voltage in a variety of ways, and eq 2 is an assumption that must be verified by measurements. In addition the change of the conduction band, and the variations of charge injection, that occur when we compare several DSC with different dyes affect the performance in ways that cannot be discriminated by inspection.

A systematic analysis is possible however, by a combined analysis of current−potential data and impedance data. We have developed a procedure that treats both sets of data simultaneously, using eqs 6 and 11. This allows checking the consistency of the application of the model, because the removal of the series resistance (voltage scale V_F) allows us to see the shape of the recombination resistance, which must follow an exponential shape as indicated by eq 11. In addition, the data of capacitance allows locating the relative position of the conduction band of the investigated cells. Then we can shift all voltages to the same reference value (voltage scale V_{ecb}, see below), and compare the recombination resistance. The cell with the larger recombination resistance in such scale has less recombination. Alternatively, we may look at j_{0k} parameter, which gives the same information.

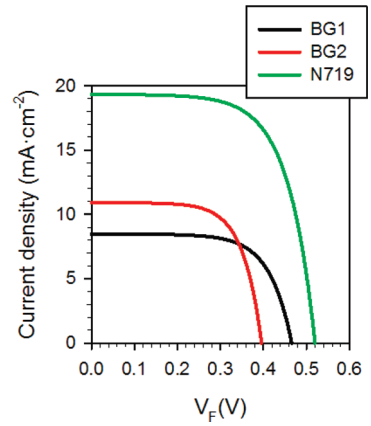

Figure 6. Simulated $j-V$ curves of DSCs sensitized with BG-1, BG-2, and N719, with respect to Fermi level voltage (without the effect of series resistance).

In either way, these results provide a quantification of recombination, in which the dependence on electron density has been factored out. This is a key step to analyze separately the causes of value of V_{oc}, i.e., the change of electron density by the influence of either more injection or less recombination. It should be emphasized that the order of recombination, β, also has a strong effect on the values of V_{oc}.

By application of this method (www.istest.eu) we obtained the parameters of recombination: β (the inverse of the ideality factor, $m = 1/\beta$), j_0 (dark current), and j_{0k} (charge-transfer constant) that are shown in Table 2. Then we can replot resistance, capacitance, and the $j-V$ curve without the contribution of series resistance, see Figure 5 and 6. We can subsequently evaluate the FF and efficiency of the cells, removing the effect of series resistance. These parameters are termed here *internal* efficiency and fill factor and are reported in the last rows of Table 2. This is a powerful tool of analysis since these last parameters provide a measure of the performance of the materials that form the photoelectrode, which is the aim of the present investigation.

In Figure 5c the voltage scale has been shifted, as explained before, so that chemical capacitances coincide. In this graph the voltage is obtained as

$$V_{ecb} = V_F - \Delta E_c \tag{12}$$

where "ecb" stands for "common equivalent conduction band" and ΔE_c is the shift of the conduction band with respect to a reference sample. In Figure 5d the recombination resistance is plotted in the same scale. In effect this procedure equalices the conduction band of titania for all the cells and allows comparison of the charge-transfer rate. It is observed in Figure 5d that at low voltage all dyes show similar charge-transfer resistance; although N719 presents less recombination. When the forward voltage increases and we get into the maximum power point and close to open circuit voltage, the recombination resistance is similar for N719 and BG-1 and larger than in BG-2. This trend is well correlated with the calculated parameters obtained with the simulation (Table 2), where it is clearly observed that j_{0k} (recombination rate constant) is higher for the large dye molecule (BG-2). Therefore, the higher performance for the BG-1 organic dye, although the light harvesting is lower than BG-2, occurs because the recombination rate is similar to that of the commercial dyes like N719 and inferior to the longer organic dye molecule (BG-2). The decrease in the overall

performance due to a fall in the V_{oc}, when the size of the organic dye (π conjugation) increases, is also reported in other families of organic dyes.[28,31,39]

In Figure 6, it is observed the "true" diode curves of the different DSC investigated, when the effect of series resistance is removed. There is obviously an enhancement of FF, that shows the potential for improvement of conversion efficiency of the cell (see the internal FF and efficiency values in Table 2), with the same values of V_{oc} and j_{sc} that have been measured. It is seen that the apparently defective $j-V$ curve for standard N719 in Figure 4 is an effect of the high series resistance; the curve looks worse than those of the organic dyes as an effect of the higher current density. It should be also emphasized, as already discussed above, that the V_{oc} of the N719 is relatively low because the electrolyte used is designed to optimize the performance of the BG dyes, which requires the position of conduction band of titania to be low.

In comparison of the performance of the two organic dye sensitizers, a trade-off is observed between enhanced photocurrent and reduced photovoltage when the number of conjugated units increases, and since the electrolyte conditions are identical, this should be related with the role that the organic dye structure plays in the charge recombination process in the DSC. Different suggestions have been reported in the literature concerning the increase of recombination, including dye interaction with I_3^-,[40] lower reorganization energy for organic dyes,[31] or possible electrostatic effects induced by the dye structure.[29] Nevertheless one effect that could significantly increase the overall recombination is the recombination thought the dye cation. While this is usually negligible for N719 and related dyes, it may become a relevant factor in organic dye molecules with a long conjugated chain. Figure 3 indicates that the HOMO level for BG dyes is distributed along the bridge part of the molecule, close to the anchoring group and indeed close to the titania surface. In addition it was reported for different organic dyes families that when the length of the bridge increases, more conjugated dye structures (i.e., larger dye structure) form less tightly packed dye layers[28] on the titania surface. This facilitates bending of the dye molecule which increases the proximity of the HOMO level to the titania surface, and improves the probability of back electron transfer to the oxidized dye molecule. Our observations indicate that BG-2 dye (the largest one, with two thiophenes units) presents higher recombination that BG-1 (with one thiophene unit) which in turn shows similar recombination as the commercial dye N719. We suggest that the observed increase of the recombination for large molecule organic dye is related with an increase in the recombination thought the dye cation. This effect has been observed in our previous work for different organic dye families.[31]

Conclusion

A family of organic dyes based on thiophene units functionalized unsymmetrically by *N*-aryl carbazole, showing high absorption in the visible region, has been synthesized and their application in dye solar cells was studied. The increase of π-conjugation in the dye molecule provides a broader spectral response, an injection current increase, and an increase of the recombination occurs in the solar cell, decreasing the V_{oc}. With a simulation treatment combining the IS and $j-V$ data it is determined that BG-2 presents more recombination but the efficiency is still higher due to the larger injection current. The increase in the recombination is attributed to an enhancement of the recombination through the dye cation due to a distribution of the HOMO level near to the titania surface, combined with the fact that when the dye molecule increases, the dye anchoring forms less tightly packed layers, increasing the probability of the bending of the molecule on the titania surface.

Acknowledgment. We are thankful for financial support from Ministerio de Cíencia e Innovación under Projects HOPE CSD2007-00007 and MAT2007-62982 and Generalitat Valenciana under Project PROMETEO/2009/058. We also acknowledge financial support from State Planning Organization of Turkey (DPT).

Supporting Information Available: Detailed synthesis description and characterization of two new carbazole dyes are reported. Injection and recombination processes are explained as a function of the energetic, a complete study about increasing injection upon lowering the conduction band of titania in a DSC. This material is available free of charge via the Internet at http://pubs.acs.org.

References and Notes

(1) O'Regan, B.; Grätzel, M. *Nature* **1991**, (353), 737–740.
(2) Kay, A.; Nazeeruddin, M. K.; Rodicio, I.; Humphry - Baker, R.; Muller, E.; Linska, P.; Vlachopoulus, N.; Grätzel, M. *J. Am. Chem. Soc.* **1993**, (115), 6382–6390.
(3) Rotzinger, F. P.; Pechy, P.; Nazeeruddin, M. K.; Kohle, O.; Zakeeruddin, S. M.; Humphry - Baker, R.; Grätzel, M. *J. Am. Chem. Soc.* **1995**, 65.
(4) Gao, F.; Wang, Y.; Shi, D.; Zhang, J.; Wang, M.; Jing, X.; Humphry-Baker, R.; Wang, P.; Zakeeruddin, S. M.; Gratzel, M. *J. Am. Chem. Soc.* **2008**, *130*, 10720–10728.
(5) Ito, S.; Wang, Q.; Grätzel, M.; Fabregat-Santiago, F.; Mora-Seró, I.; Bisquert, J.; Bossho, G.; Imai, H. *J. Phys. Chem. B* **2006**, *110*, 19406.
(6) Papageorgiou, N.; Athanassov, Y.; Armand, M.; Bonhote, P.; Pettersson, H.; Azam, A.; Gratzel, M. *J. Electrochem. Soc.* **1996**, *143*, 3099–3108.
(7) Wang, P.; Zakeeruddin, S. M.; Moser, J.-E.; Humphry-Baker, R.; Gratzel, M. *J. Am. Chem. Soc* **2004**, *126*, 7164–7165.
(8) Schmidt-Mende, L.; Bach, U.; Humphry-Baker, R.; Horiuchi, T.; Miura, H.; Ito, S.; Uchida, S.; Grätzel, M. *Adv. Mater.* **2005**, *17*, 813–815.
(9) Lupo, D.; Bach, U.; Comte, P.; Moser, J.-E.; Weissortel, F.; Salbeck, J.; Spreitzer, H.; Gratzel, M. *Nature* **1998**, *395*, 583–585.
(10) Hagen, J.; Wchaffrath, S.; Otschik, P.; Fink, R.; Bacher, A.; Schmidt, H.-W.; Haarer, D. *Syn. Metals.* **1997**, *89*, 215–220.
(11) Kim, S.; Lee, J. K.; Kang, S. O.; Ko, J.; Yum, J. H.; Fantacci, S.; De Angelis, F.; Di Censo, D.; Nazeeruddin, M. K.; Grätzel, M. *J. Am. Chem. Soc.* **2006**, *128*, 16701–16707.
(12) Edvinsson, T.; Hagberg, D. P.; Marinado, T.; Boschloo, G.; Hagfeldt, A.; Sun, L. *Chem. Commun.* **2006**, *21*, 2245–2247.
(13) Hara, K.; Sato, T.; Katoh, R.; Furube, A.; Yoshihara, T.; Murai, M.; Kurashige, M.; Ito, S.; Shinpo, A.; Suga, S.; Arakawa, H. *Adv. Funct. Mater.* **2005**, *15*, 246–252.
(14) Kitamura, T.; Ikeda, M.; Shigaki, K.; Inoue, T.; Anderson, N. A.; Ai, X.; Lian, T.; Yanagida, S. *Chem. Mater.* **2004**, *16*, 1806–1812.
(15) Marinado, T.; Hagberg, D. P.; Karlsson, K. M.; Nonomura, K.; Qin, P.; Boschloo, G.; Brinck, T.; Hagfeldt, A.; Sun, L. *J. Org. Chem.* **2007**, *42*, 9550.
(16) Hagberg, D. P.; Yum, J. H.; Lee, H.; De Angelis, F.; Marinado, T.; Karlsson, K. M.; Humphry-Baker, R.; Sun, L.; Hagfeldt, A.; Gratzel, M.; Nazeeruddin, M. K. *J. Am. Chem. Soc.* **2008**, *130*, 6259–6266.
(17) Qin, H.; Wenger, S.; Xu, M.; Gao, F.; Jing, X.; Wang, P.; Zakeeruddin, S. M.; Gratzel, M. *J. Am. Chem. Soc.* **2008**, *130*, 9202–9203.
(18) Hara, K.; Sato, T.; Katoh, R.; Furube, A.; Ohga, Y.; Shinpo, A.; Suga, S.; Sayama, K.; Sugihara, H.; Arakawa, H. *J. Phys. Chem. B* **2003**, *107*, 597.
(19) Samaya, K.; Hara, K.; Arakawa, H.; Ohga, Y.; Shinpo, A.; Suga, S. *Chem. Commun.* **2001**, *6*, 569–570.
(20) Miura, H.; Hara, T.; Uchida, S. *Chem. Commun.* **2003**, 3036–3037.
(21) Horiuchi, T.; Miura, H.; Sumioka, K.; Uchida, S. *J. Am. Chem. Soc.* **2004**, *126*, 12218–12219.
(22) Daibin, K.; Satoshi, U.; Robin, H. B.; Shaik, M. Z.; Gratzel, M. *Angew. Chem Int. Ed* **2008**, *47*, 1923–1927.
(23) Ho Lee, J.; Hwang, S.; Park, C.; Lee, H.; Kim, C.; Park, C.; Lee, M. H.; Lee, W.; Park, J.; Kim, K.; Park, N. G.; Kim, C. *Chem. Commun.* **2007**, *488*, 7–4889.
(24) Fabregat-Santiago, F.; Bisquert, J.; Palomares, E.; Otero, L.; Kuang, D.; Zakeeruddin, S.; Gratzel, M. *J. Phys. Chem. C* **2007**, *111* (17), 6550–6560.

(25) Bisquert, J.; Mora-Seró, I. *J. Phys. Chem. Lett.* **2010**, *1*, 450.
(26) Villanueva-Cab, J.; Oskam, G.; Anta, J. A. *Sol. Energy Mater. Sol. Cells* **2010**, *94*, 45.
(27) Jennings, J. R.; Wang, Q. *J. Phys. Chem. C* **2010**, *114*, 1715.
(28) Marinado, T.; Nonomura, K.; Nissfolk, J.; Karlsson, M. K.; Hagberg, D. P.; Sun, L.; Mori, S.; Hagfeldt, A. *Langmuir* **2009**, *26* (4), 2592–2598.
(29) Miyashita, M.; Sunahara, K.; Nishikawa, T.; Uemura, Y.; Koumura, N.; Hara, K.; Mori, A.; Abe, T.; Suzuki, E.; Mori, S. *J. Am. Chem. Soc.* **2008**, *130*, 17874.
(30) Gibson, V. C.; Spitzmesser, S. K.; White, A. J.; Williams, D. J. *Dalton Trans.* **2003**, *27*, 2718.
(31) Barea, E.; Caballerro, R.; Fabregat-Santiago, F.; De la Cruz, P.; Langa, F.; Bisquert, J. *ChemPhysChem* **2009**, *11* (1), 245–250.
(32) O'Regan, B.; Durrant, J. R. *Acc. Chem. Res.* **2009**, *42* (11), 1799–1808.
(33) Bisquert, J. *J. Phys. Chem. B* **2002**, *106* (2), 325–333.
(34) Fabregat-Santiago, F.; H. R.; Zaban, A.; Garcia-Cañadas, J.; García-Belmonte, G.; Bisquert, J. *Phys. Chem. Chem. Phys.* **2006**, *8*, 1827–1833.
(35) Bisquert, J.; Fabregat-Santiago, F.; Mora-Seró, I.; Garcia-Belmonte, G.; Giménez, S. *J. Phys. Chem. C* **2009**, *113* (40), 17278–17290.
(36) Fabregat-Santiago, F.; Bisquert, J.; Garcia-Belmonte, G.; G., B.; Hagfeldt, A. *Sol. Energy Mater. Sol. Cells* **2005**, *87*, 117–131.
(37) Hara, K.; Sato, T.; Katoh, R.; Furube, A.; Yoshihara, T.; Murai, M.; Kurashige, M.; Ito, S.; Shinpo, A.; Suga, S.; Arakawa, H. *Adv. Funct. Mater* **2005**, *15*, 246–252.
(38) Caballero, R.; Barea, E.; Fabregat-Santiago, F.; de la Cruz, P.; Márquez, L.; Langa, F.; Bisquert, J. *J. Phys. Chem. C* **2008**, *112* (47), 18623–18627.
(39) Li, R.; Lv, X.; Shi, D.; Zhou, D.; Cheng, Y.; Zhang, G.; Wang, P. *J. Phys. Chem. C* **2009**, *113* (17), 7469–7479.
(40) Reynal, A.; Forneli, A.; Martinez-Ferrero, E.; Sanchez-Diaz, A.; Vidal-Ferran, A.; O'Regan, B. C.; Palomares, E. *J. Am. Chem. Soc.* **2008**, *130*, 13558–13567.

JP1055842